The SAT protein of porcine parvovirus accelerates viral spreading through irreversible ER stress induction

István Mészáros[1#], Renáta Tóth[1], Ferenc Olasz[1], Peter Tijssen[2], Zoltán Zádori[1]

[1]Institute for Veterinary Medical Research, Centre for Agricultural Research, Hungarian Academy of Sciences, Budapest, Hungary.

[2]INRS-Institut Armand-Frappier, Université du Québec. Québec, Canada.

Running Head: The SATp induces irreversible ER stress

#Address correspondence to István Mészáros: meszaros.istvan@agrar.mta.hu

Abstract

The SAT protein of porcine parvovirus (PPV) accumulates in the endoplasmic reticulum (ER) and SAT deletion induces "slow spreading" phenotype. The in vitro comparison of the wild type Kresse strain and its SAT$^-$ knockout mutant revealed that prolonged cell integrity and late viral release are responsible for the slower spreading of the SAT$^-$ virus. During PPV infection, regardless of the presence or absence of SATp, the expression of downstream ER stress response proteins (Xbp1 and CHOP) was induced. However, in the absence of SATp, significant differences were detected in the quantity and the localization of CHOP, suggesting a role of SATp in the induction of irreversible ER stress in infected cells. The involvement of irreversible ER stress induction in PT cell necrosis and the viral egress was confirmed by treatment of infected cells by ER stress inducing chemicals (MG132, DTT and Thapsigargin) that accelerated the egress and spreading both the wild type and the SAT$^-$ viruses. UV stress induction had no beneficial effect to PPV infectionunderscoring the specificity of ER stress pathways in the process. However, induction of CHOP and its nuclear translocation cannot alone be responsible for the biological effect of SAT, since nuclear CHOP could not complement the lack of SAT in a co-expression experiment.

Importance

SATp is encoded in an alternative ORF of the PPV genome. Earlier we showed that SATp of the attenuated PPV-NADL-2 strain accumulates in the ER and accelerates virus release and spreading. Our present work revealed that "slow spreading" is a general feature of the SAT^- PPV viruses and is the consequence of prolonged cell integrity. PPV infection induced ER stress in the infected cells regardless of SATp presence, as demonstrated by the morphological changes of the ER, and expression of the stress response proteins XBP1 and CHOP. However, the presence of SATp made the ER stress more severe and accelerated the cell death during infection as shown by the higher expression rate and the alteration of the localization of CHOP. The beneficial effect of irreversible ER stress on PPV spread was confirmed by the treatment of the infected cells with ER stress inducing chemicals.

Introduction

Porcine parvovirus (PPV) belongs to the species *Ungulate protoparvovirus 1* in the genus *Protoparvovirus*. It is the causative agent of the SMEDI syndrome (stillbirth, mummification, embryonic death, infertility) in swine (1).

A highly pathogenic strain was isolated by Kresse with broad tissue tropism in the 1980s (2, 3). The Kresse strain-infected piglets showed atypical signs of PPV infection, including necrotic lesions (4) on the lips, snout, tongue and foot.

The PPV single-stranded genome contains two major open reading frames (ORFs) and one short, genus-specific ORF. The upstream major ORF encodes two non-structural proteins (NS1 and NS2). The NS1 has helicase and nickase activities and it can induce apoptosis (5, 6) and cell lysis (7). The NS2 protein is translated from an alternatively spliced RNA (8). The downstream major ORF encodes a nested set of three C-terminally identical structural proteins (VP1-3). A Ca-dependent phospholipase A2 (PLA2) enzyme located in the unique N-terminal region of VP1 (9) is necessary for viral infectivity.

The short genus-specific ORF overlaps with the 5' end of the ORF of VP2 protein in all *Protoparvovirus* genomes and it encodes a small alternatively translated protein (SATp) (10). The SATp contains a single membrane-spanning α-helix and it localizes in the endoplasmic reticulum-nuclear membrane network. The knockout SAT^- mutant of the attenuated NADL-2 strain of PPV shows a "slow-spreading" phenotype in cell culture. Based on *in vitro* complementation studies it was presumed that the function of the SATp is to induce endoplasmic reticulum (ER) stress to facilitate cell lysis (10).

The ER plays a key role in protein folding and maturation. The immature proteins enter the ER lumen, where they are folded by molecular chaperons (e.g. Grp78, Grp 94, calnexin) and protein-folding enzymes like calreticulin and protein disulphide isomerase (11). At the

end of the maturation process only the correctly structured proteins are transported to destination sites with ER vesicles (12). Incorrectly folded proteins accumulate in the ER lumen causing ER stress. Multiple transmembrane sensors of signalling pathways detect the ER stress including the protein kinase R-like kinase (PERK) (13), the inositol-requiring kinase/endoribonuclease 1 (IRE1) and ATF6 (14).

IRE1 has endoribonuclease and serine/threonine protein kinase activity and its signalling pathway represents the most conserved element of the ER stress response (15, 16). After activation, the IRE1 cuts out a 26 base pair length section from the mRNA of the X box-binding protein 1 (Xbp1) that leads to a frame shift and a spliced Xbp1 protein (Xbp1s). Xbp1s is transported to the nucleus and regulates the expression of genes contributing to protein folding, glycosylation and ER membrane biogenesis (17, 18).

The activated PERK phosphorylates the eukaryotic translation initiation factor 2α (eIF2α), that inhibits the translation of most mRNAs (19), thus reducing the protein load and easing ER stress (20, 21). At the same time the translation rate of some ER stress-related proteins – including the Activated Transcription Factor 4 (ATF4) – increases. ATF4 induces the translation of genes that regulate amino acid biosynthesis and transport (22). One of the ATF4-stimulated genes is the C/EBP homologous protein (CHOP) (23). Under prolonged or severe ER stress CHOP irreversibly triggers programmed cell death (24, 25).

In the present study, we show that wild-type (wt) PPV infection induces irreversible ER stress whereas the loss of SATp through mutations lessens this ER stress and leads to reduced apoptosis and cell lysis in virus-infected cells. ER stress-inducing drugs can compensate for the loss of SAT *in vitro*, and they accelerate the egress of the wt PPV. This process seems to be ER stress specific, since UV stress doesn't induce similar effect.

Materials and Methods

126 ***Cells, viruses and transfection***

127 PT cell line was used in all experiments. The cells were grown in a DMEM-based
128 medium (high glucose: 4.5 g/l, PAA) supplemented with 10% serum (Fetal Bovine Serum
129 Gold, PAA), 1% penicillin-streptomycin (PAA) and 1% sodium-pyruvate solution (Lonza) in
130 the presence of 5% CO_2 at 37°C.

131 For infection and transfection, the cells were seeded in 24-well tissue culture plates
132 (1×10^5 cell/well) and they were infected or transfected with either the wt PPV Kresse or the
133 SAT^- mutant of PPV Kresse strain at about 50% cell confluency. We used 0.01 multiplicity of
134 infection (MOI) to monitor viral spread and 3 MOI (optimal MOI to use a minimal number of
135 viruses to target the maximal number of cells) in the experiments to investigate virus release,
136 apoptosis, viability and ER-stress. Infectious titer of the viral stocks was determined as
137 described earlier (10). Data was averaged from four independent dilutions.

138 The wt and mutant viral stocks were created by transfecting PT cells with pKresse
139 (pUC19 cloned PPV Kresse virus (26)) and $pSAT^-$ plasmids, respectively. By using the
140 method described earlier, two nucleotides of pKresse (T-2842→A and T-2845→C) were
141 changed to knock out SAT and to create $pSAT^-$ (10) (Figure 1).

142 Fusion constructs alone were transfected into adherent cells using the TurboFect
143 Transfection Reagent (Thermo Scientific) following the supplier's recommendations.

144 Co-transfection of the infectious clones with fusion constructs were performed in
145 suspension cell cultures as follows. 1 µg infectious clone and 1 µg fusion construct DNA were
146 mixed with 3 µl Turbofect reagent in 100 µl DMEM and incubated for 20 min at room
147 temperature. The transfection mix was then added to 1 ml freshly trypsinized, suspended PT
148 cells ($1x10^5$ cells/ml in DMEM with 10% FBS) and incubated on a gently rocking platform
149 for 3 h at room temperature. Cells were centrifuged at 1000g for 1 min, re-suspended in 1 ml
150 fresh medium and plated in 24-well plates.

151

152 ***Fusion constructs***

153 DsRed-labelled SAT and CHOP protein constructs were created in DsRed-Monomer-
154 N1 plasmids (Clontech). The SATp and CHOP sequences were amplified by the PPV-SATf
155 (GC GGTACC ATG TGG AAC AAC ACA ACC CTA), the PPV-SATr (CG GGTACC TT
156 GAT GTA TGA GTC TTG ATG CGT), the F-CHOP-DsRed (GC AAGCTT ATG GCA GCT
157 GAG TCA TTG CCT) and the R-CHOP-DsRed (GC GGATCC CG TGC TTG GTG CAG
158 ATT AAC CAT) primers, and by Phusion Hot Start DNA polymerase. To get the template for
159 CHOP, total RNA was purified with RiboZol (Amresco), and reverse transcribed with
160 Superscript III (Thermo Fisher Scientific) using the R-CHOP-DsRed primer according to the
161 manufacturer's recommendation.

162 The isolated PCR fragments and the vector were digested with KpnI or HindIII and
163 BamHI restriction enzymes and were ligated with T4 ligase (Thermo Scientific).

164

165 ***Immunofluorescence staining***

166 For immunofluorescence (IF) staining the cells were plated on coverslips. They were
167 fixed at the appropriate time with 3% formaldehyde and incubated for 30 min at room
168 temperature. After two washing steps (1.5 g bovine serum albumin dissolved in 300 ml
169 1×PBS) they were permeabilized using 1% Triton-X (Sigma-Aldrich). After 15 min the cells
170 were washed twice, 5% inactivated horse serum (diluted in PBS) was loaded into the wells
171 and the plate was incubated for 30 min at room temperature. After two washings the cells
172 were exposed to primary antibodies (3C9 (CRL-17, ATCC) mouse anti-PPV capsid-specific
173 monoclonal antibody, mouse anti-CHOP (Thermo Scientific), rabbit anti-Xbp1 (Santa Cruz
174 Biotechnology and sera of the PPV infected swine) for 60 min at room temperature. After
175 further washings the cells were incubated with their respective secondary antibodies (CF594

anti-mouse, CF488 anti-mouse, CF488a anti-rabbit or the CF 586 anti-swine antibodies (Biotium)) for 60 min at room temperature in the dark. After final washings the cover glasses were removed from the wells and were fixed into a slide using Fluoroshield (Sigma-Aldrich) according to the manufacturer's protocol. An Axio Observer D1 inverted fluorescence microscope (Zeiss) was used for visualization.

Fluorescent Focus growth inhibition

For finding the neutralizing concentration of the 3C9 monoclonal antibody, the supernatant of the 3C9 hybridoma was diluted 10× 20× 50× 100× in complete medium and 50 µl of the diluted solutions were mixed with 50 µl 0.01 MOI viral stock, then incubated for 1 hour at room temperature. After incubation 100 µl of the media containing the antibody virus complexes were loaded to 50% confluent PT cells on a 96 well plate and the cells were incubated at 37°C for viral growth. After 24 hours the cells were fixed and the progress of infection was detected with the standard IF method described above. Twenty times diluted supernatant completely blocked the PPV infection. In the next step the PT cells were infected with 50 µl low MOI viral stocks (0.01) and incubated at 37°C. After 4 hours the supernatant was removed, 50 µl medium with 20× diluted 3C9 was added, and the cells were incubated at 37°C for an additional 20 hours. After the incubation the cells were fixed and monitored for viral infection with the standard IF method.

Apoptosis and viability experiments

For the investigation of apoptosis and lysis, the cells were seeded at 50% confluency ($2{,}5x10^5$) in 24-well plates and after 3 h they were infected with viruses. Live, unfixed, infected and uninfected cells were incubated with 1µg/ml Hoechst 33342 and with 0,25 µg/ml propidium iodide at different time points (18 h-88 h p.i.) for 60 min at room temperature in

the dark. Then they were washed with PBS, examined under a microscope, and several photographs were taken from the central regions of the wells in the blue and the red channels. All cells including PI positive and apoptotic cells were counted from 3-6 photographs of each well and averaged. Pyknotic nuclei were identified by strong staining with Hoechst, fragmentation or nuclear shrinkage to 1-4 µm (27). More than a thousand cells were counted (on minimum four photos) for every time point (except when attached cell count went under 20% of the total) by two independent persons and data was averaged. The Mann-Whitney U test was applied for the statistical analysis of the data where the null hypothesis was that the two samples came from the same population.

Lysis was quantified based on lactate dehydrogenase enzyme (LDH) activity (28, 29) by a Cytotoxicity Detection KIT (Roche) following the manufacturer's instructions. The absorbance was measured in the linear range after 1:1 dilution of the supernatants with PBS by an EL×800 ELISA plate reader (Dialab GMBH., Austria) at 490 nm. Sample absorbance was calculated by subtracting the background value of the serum from the measured data.

Real-time quantitative PCR

The supernatants of the infected cells were sampled between 0 h p.i. and 84 h p.i. The viral DNAs were purified with High Pure Viral Nucleic Acid KIT (Roche) according to the manufacturer's protocol. The qPCR reaction solution (25 µl) contained 18.25 µl water, 2.5 µl 10× DreamTaq Buffer (Thermo Scientific), 0.5 µl dNTP mix (2 mM each), 1 µl template DNA from the supernatants, 0.5 µl DreamTaq DNA Polymerase (Thermo Scientific), 1.25 µl 20× EvaGreen™ Dye (Biotium), 0.5 µl forward primer (CTT TAG CCT TGG AGC CGT GGA) and 0.5 µl reverse primer (AAC TAC CCT TAC CTC TTG CTC TT) (both 20 pM/µl concentration).

225 The thermal reaction started with a pre-denaturation step at 95°C for 5 min and
226 followed by 40 cycles (denaturation at 95°C for 30 sec, annealing at 55°C for 30 sec and
227 elongation at 72°C for 50 sec) and finished with a post-elongation step at 72°C for 5 min. The
228 specificity of the qPCR was verified with melting curve analysis.
229
230 ***DNase treatment***
231 20 µl 10× DNase puffer with 25 mM $MgCl_2$ (Thermo Scientific) and 4 µl 50U/µl bovine
232 pancreatic DNase I (Roche) were added to 200 µl supernatant of the infected cells. After 90
233 min at room temperature the viral DNA was purified with High Pure Viral Nucleic Acid KIT
234 (Roche) according to the manufacturer's protocol.
235
236 ***ER stress induction***
237 The plated and infected cells (MOI: 0.01 and 3) were incubated with 20 µM MG132 or
238 10 mM DTT (dithiothreitol) at 0-5 h, 3-8 h, 5-10 h, 7-12 h p.i. or 10 µM thapsigargin at 0-2 h,
239 2-4 h, 4-6 h, 6-8 h p.i. on 37°C. After the chemical incubation period the cells were washed
240 twice and 1 ml fresh cell culture medium was added into the wells. The supernatant was
241 harvested and the cells were fixed at 24 h p.i.
242
243 ***UV stress induction***
244 The infected cells (MOI: 3) were treated with sub-lethal UV-C light (30 W light source, 50
245 cm distance) for 5 min at 0, 3, 9 and 12 h p.i. After the treatment period the cells were washed
246 twice and 1 ml fresh cell culture medium was added into the wells. The supernatant was
247 harvested at 24 h p.i. and the cells were fixed for further examinations.
248
249 **Results**

250 ***Spread of the wild type and SAT⁻ mutant PPV Kresse strains***

251 Previously, we reported that the SAT⁻ mutant of the attenuated NADL-2 strain of PPV
252 has a slow spreading phenotype (10). In the present study, our first step was to investigate
253 whether the loss of SAT causes a similar effect in the virulent Kresse strain.

254 For this purpose, first a SAT⁻ knockout mutant Kresse strain was created by eliminating
255 a potential second initiation codon of SAT (8 codons behind the initiation codon of SAT) and
256 introducing a stop codon into the SAT coding frame in the infectious clone of Kresse strain
257 without changing the protein sequence of the VP proteins (Figure 1). Then PT cells were
258 infected with the rescued SAT⁻ and wt virus at low (0.01) MOI. The differences between the
259 spreading of two virus strains were monitored by IF staining using 3C9 assembled capsid
260 sensitive primary antibody.

261 The first positive cells appeared at 12 h p.i. with both the wt and the SAT⁻ mutant virus
262 indicating similar kinetics in viral entry, decapsidation, replication, viral protein synthesis and
263 capsid assembly. The number of positive cells continuously grew until 20 h p.i. when the first
264 secondary infections could be detected in the wt virus-infected cells in the form of
265 fluorescence foci, while the first signs of re-infection were visible only at 24 h p.i. in the case
266 of the SAT⁻ mutant virus (Figure 2/A). Incubation of the low MOI virus infected cells with
267 the 3C9 neutralizing antibody abolished the appearance of large FFs (fluorescent focus) at 24
268 hours with both the wild type and the SAT⁻ viruses, proving that large FFs are indeed the
269 results of secondary viral infection. (Figure 2/B, only wild type is shown). The difference in
270 virus spreading became even more obvious as the infection progressed. At 48 h p.i., the wt
271 virus infected almost every cell, in contrast to the SAT⁻ strain. Changes in infectious titer and
272 viral copy numbers of the supernatant correlated well with the spreading pattern revealed by
273 IF staining (Figure 3/A). Thus, the loss of SATp in the pathogen Kresse strain and the
274 attenuated NADL2 strain (10) resulted in a similar phenotype.

High multiplicity infection indicated impaired egress for the SAT$^-$ Kresse strain. The copy number of the wt virus in the supernatant started increasing sharply at 20 h p.i. as a consequence of mass release of the viruses and viral DNA from a large number of infected cells (Figure 3/B). The copy number increase of the SAT$^-$ mutant virus started later (between 22 h and 24 h p.i.) and the number of viral genomes in the supernatant remained constantly under that of the wt virus. The biggest difference between the copy numbers was around 48 h p.i. and it decreased gradually until the end of the monitoring period.

DNase treatment of the supernatants revealed that the majority of the qPCR-detected viral copies in the supernatant of the infected cells came from DNase-sensitive replicative forms and partially- or non-encapsidated genome forms released, most probably, from the dying cells (Figure 3/B). The difference between the DNase-resistant copy numbers in the supernatant of the two strains decreased to minimal by the end of the monitoring period (84 h p.i.), indicating very similar amounts of packaged DNA and infectious virus production. Titering of the wt and SAT$^-$ stocks on PT cells (4.85×10^9 and 2.56×10^9) indeed revealed very similar infectious particle production. This result was also congruent with our earlier findings with the NADL2 strain and its SAT$^-$ mutants (10).

We theorized that the quicker release of the wt virus must be the consequence of earlier cell death and lysis induced by SATp in the host cell. To better understand the function of SATp, we first studied the phenotypic effects including viability, cell lysis, and apoptosis of SAT$^-$ and wt viruses on infected cells.

Cytopathogenic effects of the viral infection

First LDH release as an indicator of cell lysis was quantified from high MOI-infected cells. (30) (Figure 4/A). The released LDH level started to increase much faster (exponentially R^2: 0.9946) in wt virus-infected cells from 18 h p.i. until 48 h p.i than in SAT$^-$ infected cells,

where the increase was logarithmic (R^2: 0.9639) in this interval. Measured values reached an approximately twofold difference at 48 h p.i. in the supernatant of wt virus-infected cells. At this time-point barely any of the wt virus-infected cells remained alive while the majority of the SAT$^-$-infected cells stayed adherent (Figure 4/B). Extracellular LDH activity of SAT$^-$ infected cells started to sharply increase after 64 h and that was preceded by a rapid decrease in the attached cell count. Monitoring the attached cells with propidium iodide revealed that the membrane integrity of the SAT$^-$-infected cells was also sustained for a longer time and in more cells than that of the wt virus-infected cells (Figure 4/C) The number of pyknotic and karyorrhectic nuclei remained relatively low during the course of infection of both viruses (less than 14% and 8% in the case of wt and SAT$^-$ viruses, respectively) (Figure 4/D). Nevertheless, their rates were always higher in wt virus-infected than among SAT$^-$-virus infected cells, and the difference became and remained statistically significant ($p<0.046$) starting at 28 h p.i. Plasma membrane blebbing could hardly be seen in infected cells while their nuclei were frequently enlarged (Figure 4/E, 5).

These experiments highlight that lysis, rather than apoptosis is the main form of cell death during PPV infection in PT cells. They also reveal that the loss of SAT prolongs cell life throughout PPV infection and it decreases the number of both lysed and necrotic cells during the course of infection.

The effect of ER stress inducers

Since SATp accumulates in the ER, it seemed plausible to presume that SATp facilitates early cell death and virus release through ER stress induction. To gather evidence on the effect of ER stress on PPV egress, the influence of ER stress inducer drugs was investigated on infected cells. PT cells were infected with wt and SAT$^-$ Kresse strains at low multiplicity (MOI 0.01), and the cells were treated at different time points with 10 mM DTT,

20 μM MG132 or 10 μM thapsigargin. The cells were fixed at 20 h p.i. and monitored for the presence of plaque-like FFs of PPV by IF (Figure 5). In untreated cells at 20 h p.i. the SAT$^-$ virus does not induce FFs, only individual cells are positive for the virus.

Treatments with all ER stress inducers moderately increased the size of FFs in wt virus-infected cells, but most importantly, they also induced FFs in SAT$^-$ virus-infected cells, regardless of the starting time of the treatment. The MG132 treatment starting at 3 h p.i. gave the biggest and highest number of FFs. Under these conditions the size of the FFs of the SAT$^-$ virus was similar or even bigger than that of the wt virus in untreated cells (Figure 5).

The same treatments (10 mM DTT or 20 μM MG132) gave similar results at high multiplicity (MOI 3) infection, where the virus titer was quantified by qPCR at 24 h p.i. from the culture media (Figure 6/A). Both ER stress inducers substantially increased viral egress into the media. DTT treatment starting at 7 h p.i. had the strongest effect on wt virus release (4.41×), while the 3 h p.i. MG132 treatment induced the highest titer increase in the medium of cells infected with the SAT$^-$ virus (71.67×). Unexpectedly, almost all of the tested chemical treatments (with the exception of the 7 h p.i. DTT treatment) increased the SAT$^-$ virus titer above not only the basic wt virus titer but also that of the chemically-enhanced wt values.

Back titration of the supernatants of ER stress inducer-treated cells verified that the increase of the viral copy number correlates with the increase of the number of infectious particles in the supernatants (Figure 6/C).

To investigate the specificity of the ER stress among other stress factors to accelerate viral egress, the effect of UV radiation was also examined. Short term sub-lethal UV-C light treatment (5 min) did not change the viral copy numbers considerably, while it significantly reduced (to ~2%, $p<0.005$) the number of the infectious particles in the supernatant (Figure 6/B and C).

The results of these experiments strongly suggested that ER stress indeed facilitates the release of matured particles from infected cells, and ER stress seems to be specific in this regard because UV-C radiation is not able to induce a similar effect.

Detection of ER stress

To further clarify the relation of ER stress and SATp to the acceleration of viral egress, the pattern of ER and ER stress markers was studied in infected cells. PT cells were infected with the SAT^- and the wt Kresse strains (MOI: 3), and calreticulin as ER marker, as well as Xbp1 and CHOP as downstream ER stress response markers were monitored by IF staining. PPV infection – with or without SAT – causes condensation in the ER membranes of the infected cells. Perinuclear nodes and clots could be detected implying fragmentation and fusion of the tubular network as obvious signs of ER stress (31, 32, 33) (Figure 7). However, no significant differences were found between the wt virus- or SAT^- virus-infected cells in the starting time or in the pattern of the disintegration in attached cells.

There was also no difference between SAT^+ and SAT^- viruses until 48 hours when the reversible ER stress marker Xbp1 was monitored during viral infection (Figure 8/A). Xbp1 was mainly detected in the nuclei of infected cells with the earliest detection time of about 14 h p.i. The presence of the protein was temporary, its level peaked sharply at 16-18 h p.i., when around 95% of the infected cells showed positivity. After that it rapidly declined: at 20 h p.i. the Xbp1 could only be detected in less than 5% of the cells. Low level Xbp1 expression was detected again in SAT^- virus infected cells at 60 h p.i. However that was most probably the consequence of ER stress induced by nutrient-starvation (34) because similar level Xbp1 expression was also visible in non-infected cells at the same time (Figure 8/C).

Among the monitored markers, only the irreversible ER stress marker CHOP showed a difference between wt and SAT^- virus infection (Figure 8/B). In the wt virus-infected cells

CHOP was detected first at 22 h p.i. in around 20% of the cell nuclei. Its expression plateaued at 24 h p.i. with 75% positivity in the infected cells, and remained relatively unchanged until 36 h p.i.. After 36 hours very few attached infected cells showed positivity to CHOP. Although in SAT$^-$ virus-infected tissue CHOP was also detected at 22 h p.i. in around 20% of the nuclei of infected cells, but instead of nuclear localization it was detected perinuclearly in the cytoplasm. It also plateaued at 24 h p.i. but only with 41% positivity in the cells; this value essentially remained unaffected until 36 hours in attached cells and the perinuclear localization of the protein did not change either. CHOP could not be detected after 48 hours in SAT$^-$ virus-infected cells.

These experiments show that PPV infection induces ER stress regardless of the presence or absence of the SATp. However, the wt virus expressing the SATp is able to activate the expression of CHOP in significantly more cells than the SAT$^-$ virus, and SATp also influences the localization of cell death triggering CHOP in infected cells.

Since chemical ER stress inducers were able to compensate for the loss of SAT, their effect on the induction of ER stress markers was also monitored. As expected, the chemicals induced Xbp1 and CHOP expression in the treated cells (Figure 8/D). CHOP expression could be detected in 100% of the treated cells at 18 h and 8 h after the beginning of MG132 and DTT treatment, respectively. However, the chemical treatments always triggered the nuclear localization of CHOP similarly to wt virus infection but contrary to SAT$^-$ virus infection. Sub-lethal UV treatment of the PT cells did not induce either Xbp1 or CHOP expression.

These findings gave additional support to the possible role of nuclearly localized CHOP in the acceleration of cell lysis.

Effect of the cloned SAT protein in PT cells

To further explore the role of SATp in the induction of ER stress markers, a SAT-DsRed fusion protein-expressing vector was transfected into PT cells. Transfected cells were fixed in the 16-48-hour post transfection period every four hours and examined for XBP1 and CHOP expression by IF. Neither protein was induced in SAT-expressing cells during the monitoring period (data not shown), despite the fact that in their ER similar morphological alterations (condensation in the perinuclear region) could be detected as in infected cells (Figure 9). During the monitoring period, the SATp always co-compartmentalized with calreticulin (Figure 9). Furthermore, the SAT-DsRed protein induced apoptosis (Figure 9) in the late phase of the transfection (from 30 h post transfection). After 48 h p.t., only very few SAT-DsRed-expressing cells could be detected in the transfected wells while cells expressing the control DsRed protein remained viable and detectable even after 90 h p. t.

These experiments indicate that SATp alone is toxic and its accumulation has an effect on the morphology of the ER. However, without the other viral proteins SATp is not able to activate either XBP1 or CHOP expression.

Effect of the nuclear CHOP on viral spread

Since the presence of the nuclearly localized CHOP in the infected cells showed strong correlation with the accelerated viral egress, we further studied the role of CHOP in the process. We cloned the porcine CHOP and made a construct constitutively expressing the porcine CHOP-DsRed fusion protein. Many studies reported that transiently expressed mammalian CHOP from a transfected plasmid accumulates in the nucleus. Indeed, the transfections of our construct alone or together with the pSAT$^-$ or the pKresse infectious clones resulted in the nuclear localization of the CHOP-DsRed protein (Figure 10/A). The CHOP-DsRed protein proved to be functionally active because it could induce apoptosis in the transfected cells as early as 18 h p.t. (Figure 10/B) and it killed almost all transfected cells

at 48 h p.t. (data not shown). However, when the CHOP-DsRed expressing construct was co-transfected with pSAT$^-$ it did not increase the size of FFs in contrast to the SAT-DsRed expressing construct that readily induced large size FFs (compared to the size of FFs in cells transfected with the pSAT$^-$ plasmid only) (Figure 10/C). This experiment revealed that nuclear CHOP alone is not able to induce such transcriptional changes in the nucleus that would accelerate cell lysis and viral spread.

Discussion

Quantification of the medium of high and low MOI-infected cells by qPCR and titration revealed that SATp induces early viral release but does not increase the final virus production (Figure 3).

The dynamics of the viral titer increase is quite different in the medium of high and low MOI infected cells. At low MOI infection orders of magnitude differences can be detected between the mutant and the wild type virus during the 40-64th hours of the infection (Figure 3/A). The accumulating effect of the 3-4 hour delays in *first* viral release in every consecutive replicative cycles, together with the sharp decrease of the dividing cells that support parvoviral replication after 28 h p.i. (the cell number grows to more than 2.5 of the seeding number in the first 28 hours (Figure 4/B), while in the next 60 hours the growth rate is drastically reduced) can provide a plausible explanation to the phenomenon.

It may look surprising that at high MOI infection, when *all* of the cells are infected at the same time, the difference is much smaller. However, we can only expect to see orders of magnitude differences if any or both of the following premises are fulfilled: (i) one of the viruses produces much more progeny than the other in the cells or (ii) at a given time point orders of magnitude more cells lyse and release progeny viruses. We showed in an earlier paper as well (10) that SAT$^-$ and wild type viruses produce equal amounts of progeny viruses.

449 In order for the second premise to be true, magnitudes of more cells should be dying among
450 SAT$^-$ than wild type virus infected cells at any given time, that is obviously not the case. The
451 biggest differences in DNase-resistant viral copy numbers (6.5×) can be seen around 48 h p.i.
452 (Figure 3/B), after 95% of the wild type infected cells detached and started to lose their
453 integrity (indicated by attached cell count at 42 h p.i.) and they lyse en mass (see jumps in
454 LDH activity at 48-64 h p.i). At the same time around 15% of the SAT- cells are detached and
455 lysed (Figure 4). The 95% versus 15% is a big difference regarding detached cell numbers,
456 however their ratio is only 6.33×, which is a pretty good match of the measured 6.5×
457 difference in viral copy number in the media, given that all the dead cells produced equal
458 amount of viruses.

459 Interestingly, wild type virus infected cells release more DNase-sensitive viral DNA
460 than SAT$^-$ virus infected cells (3/B). Since DNA is a potent immunostimulator acting through
461 several DNA-sensing receptors (35), this phenomenon may have potential therapeutic
462 significance for the development of oncolytic parvoviruses (36).

463 It was reported earlier that MVM and H1-PV, close relatives of PPV, are actively
464 transported in vesicles from the nucleus to the cell periphery and released into the culture
465 medium (37). However, we were not able to detect any assembled capsid in the cytoplasm of
466 either wt or SAT$^-$ virus-infected cells at low (0.01) or even at high (3) MOI infection (Figures
467 2 & 5) until the cells started to lyze en masse (wt 40 h p.i.; SAT$^-$ virus 64 h p.i. at 3 MOI) and
468 large amount of virus was released into the culture media which re-infected the remaining
469 cells. This observation suggests that vesicular transport does not play a significant role in the
470 egress of PPV, at least not in PT cells.

471 Members of the *Protoparvovirus* genus can induce either necrosis or apoptosis,
472 depending on the virus, and on the cell type (38). Parvovirus infection is also able to activate
473 early apoptotic events that do not go to completion and can lead to necrotic cell death as

474 demonstrated by H-1 infection in HeLa and P1 cells. In case of PPV it was reported that the
475 YL strain induces apoptosis in ST and PK-15 cells and in late phase of the infection (60 h p.i.)
476 the number of apoptotic cells can reach 50% (39, 40). In contrast, during Kresse strain
477 infection in PT cells the number of apoptotic cells remained low as indicated by the number
478 of pyknotic and karyorrhectic nuclei, and it never exceeded 14% regardless of the presence or
479 absence of SATp. Since subtle mutations of the PPV capsid can modify interactions with host
480 factors and change the cytopathic effect of the virus (26, 41) it is hard to pinpoint whether the
481 viral strains or the cell lines used are responsible for the observed differences.

482 It is worth mentioning that neither pyknosis nor karyorhexis are exclusive
483 characteristics of apoptosis: they are frequently detected in non-apoptotic, necrotic cells as
484 well (necrotic pyknosis). Strikingly we never detected any nuclear fragmentation inside an
485 infected cell with well-defined nuclear boundary. Apoptotic nuclei were readily produced in
486 SAT- and CHOP-expressing cells (Figure 9, 10) and they were also demonstrated in
487 parvoviral NS1-transfected cells (42). Our findings suggest that cell death in PT cells during
488 PPV infection is not characteristically apoptotic even if apoptotic pathways are involved as
489 indicated by CHOP induction. Swelling of the infected nuclei, lack of blebbing, early cell
490 membrane failure as indicated by PI uptake, rapid LDH and free viral DNA release all point
491 toward necrosis as the main form of cell death in PT cells during PPV infection.

492 ER stress inducers could mimic the effect of SATp. To minimize the chance that the
493 observed result is the consequence of unknown side effects, three differently acting chemicals
494 (DTT, MG132 and thapsigargin) that are commonly used for the activation of the unfolded
495 protein response (UPR) (43, 44, 45) have been tested. DTT reduces the disulphide bonds (46)
496 of the proteins and results in the accumulation of un- or misfolded proteins. MG132 is a
497 proteasome-specific protease inhibitor (47) that blocks the degradation of proteins, while
498 thapsigargin is a sarco-endoplasmic reticulum Ca^{2+}-ATPase inhibitor and it increases the free

499 Ca^{2+} concentration in the cytosol (48). Thapsigargin was shown to inhibit parvoviral
500 infection. Boisvert et al. (49) also showed that sustained MG132 treatment starting at the early
501 stage of the PPV NADL-2 infection blocks infection (0-20 h p.i. treatment ~100% inhibition,
502 8-20 h p.i. treatment ~50% inhibition). Similar MG132 treatment induced very similar effects
503 at PPV Kresse infection as we detected it by monitoring low MOI infection (not shown). In
504 fact all tested inducers had an inhibitory effect on viral infection when were applied at higher
505 concentration or over an extended period of time. However, they enhanced the spreading of
506 the SAT^{-} strain at the low multiplicity infection (MOI: 0.01) and two of them increased viral
507 release at high MOI (thapsigargin has not been tried) under the applied conditions. This
508 happened despite the fact that DTT and thapsigargin were visibly toxic to the cells.
509 Obviously, the concentration and the timing of the treatments fundamentally influenced the
510 outcome of the experiments, indicating a delicate balance between the opposing effects of
511 these chemicals on the infectious process. Many chemicals can be used to demonstrate a
512 negative effect on parvoviral infection. The special feature of this work is that it demonstrates
513 a positive effect on this process by using inhibitors.

514 All inducers in the applied concentration switched on XBP1 and CHOP expression that
515 led to the death of 100% of the cells in 48 h. Interestingly, switching UPR early on was not
516 only beneficially influencing viral egress as indicated by the titer of the treated high MOI-
517 infected cells (Figure 6) but, at least seemingly, it did not have a large negative effect on
518 parvoviral entry and replication, otherwise second cycle replication and the increase of FFs
519 could not have been detected at low MOI-infected cells already in the stage of UPR (Figure
520 5).

521 UV stress did not produce any enhancement on PPV release, and it did not activate
522 XBP1 and CHOP expression (Figure 8/C). Earlier it was shown that pre-treatment of cells
523 with UV light facilitates the replication of AAV (50, 51), however, it does not significantly

affect the replication of H-1 parvovirus, though it increases the mutation rate of the virus in a dose-dependent fashion (52). We found that sub-lethal UV stress applied to the cells after infection does not significantly affect PPV virus output, but – not surprisingly – considerably (~50x) reduces the infectious titer of the progeny viral stocks (Figure 6/C). The probing of different stress factors strongly suggested that ER stress indeed facilitates the release of matured particles from infected cells, and ER stress seems to be specific in this regard, because UV-C radiation is not able to induce a similar effect.

Our experiments with wt and SAT$^-$ viruses revealed that PPV similarly to numerous other viruses from different viral families (53, 54, 55, 56, 57) induces ER stress and UPR in the infected cells as demonstrated by the morphological changes of the ER and expression of XBP1 and CHOP (58). It is suspected that different localisation of the CHOP depends on the state of the cells and the intensity of the stress effect (59). In wt virus-infected cells CHOP was detected in the nuclei of the majority of the cells indicating severe ER stress, while in SAT$^-$ virus-infected cells CHOP was also expressed, but to a lesser extent (41% versus 76% of the cells) and its localization remained perinuclear (Figure 8/B). It is generally accepted that nuclear CHOP is one of the most important mediators of cell death during ER stress (25, 58). CHOP is a transcriptional activator of several pro-apoptotic proteins (e.g. GADD34, DR5, Ero1α) and inhibits the transcription of the anti-apoptotic Bcl-2 (60, 61). On the other hand, it was also shown in mouse embryo fibroblasts that forced expression of CHOP alone or together with ATF4 does not increase the expression of cell death-related genes, only sensitizes to ER stress-induced cell death (62). Besides CHOP expression, increased protein synthesis and oxidative stress were required to induce cell death. In our case, expressed porcine CHOP was clearly detrimental to PT cells causing nuclear fragmentation and cell death (Figure 10/B) in the majority of cells at 48 h post transfection. These data suggest that

548 the outcome of CHOP expression can depend on the cell type and on the actual status of the
549 cell.

550 The presence of SATp clearly influences the localization of CHOP and the outcome of
551 the ER stress response during PPV infection. It is likely that SATp increases the stress effect
552 in the infected cells, that leads to the nuclear accumulation of the CHOP and to the induction
553 of pro-apoptotic or other pathways that accelerate the death of the infected cells. The effect of
554 overexpressed SATp in transfected cells supports this theory. SATp alone is able to change
555 the morphology of the ER and can induce apoptosis (Figure 9). It is clear that the influence of
556 SATp on the activation and localization of CHOP cannot be direct, because by itself it cannot
557 induce CHOP expression (data not shown). It occurred to us that the DsRed tag can influence
558 the functional interactions of SATp, but we transfected tagless SATp expressing plasmids into
559 PT cells and were not able to detect XBP1 and CHOP expression either. The functionality of
560 SAT-DsRed is further supported by the fact that in a co-transfection experiment the protein
561 could complement the missing function of native SATp (Figure 10/C).

562 However, no matter which way SATp stimulates the expression of CHOP, it seems that
563 the induction of this protein and its nuclear localization cannot alone be responsible for the
564 biological effect of SATp, since nuclear CHOP could not complement the lack of SATp in a
565 co-expression experiment (Figure 10/C). Since severe ER stress emulates the effect of SATp,
566 one of the most likely mechanism of action of SATp is that in the ER it influences protein
567 interactions, which make the UPR response more severe. This process may lead to the
568 activation of the PERK-eIF2α-ATF4-CHOP pathway where one or more of the proteins
569 upstream of CHOP also induce alternative pathways. These may supplement the effect of
570 CHOP leading to early cell death. In an alternative scenario, SATp may induce other ER
571 stress response pathway/s beside UPR (e.g. ER overload response), and this effect alone or
572 synergistically with the CHOP pathway couse early cell death.

Funding information

The study was supported by the Hungarian Scientific Research Fund (K108607) and National Research, Development and Innovation Office (K119381). The funders had no role in study design, data collection and interpretation, or the decision to submit the work for publication.

References

1. **Johnson RH, Collings DF.** 1969. Experimental infection of piglets and pregnant gilts with a parvovirus. Vet Rec. **85**(16): 446–447.
2. **Choi CS, Molitor TW, Joo HS, Gunther R.** 1987. Pathogenicity of a skin isolate of porcine parvovirus in swine foetuses. Vet Microbiol. **15**: 19–29.
3. **Oraveerakul K, Choi CS, Molitor TW.** 1993. Tissue tropisms of porcine parvovirus in swine. Arch of Virol. **130**: 377-389.
4. **Kresse JI, Taylor WD, Stewart WW, Eernisse KA.** 1985. Parvovirus infection in pigs with necrotic and vesicle-like lesions. Vet Microbiol. **10**: 525–531.
5. **Rayet B, Lopez-Guerrero JA, Rommelaere J, Dinsart C.** 1998. Induction of programmed cell death by parvovirus H-1 in U937 cells: connection with the tumor necrosis factor alpha signalling pathway. J. Virol. **72**: 8893–8903.
6. **Sol N, Le Junter J, Vassias I, Freyssinier JM, Thomas A, Prigent AF, Rudkin BB, Fichelson S, Morinet F.** 1999. Possible interactions between the NS-1 protein and tumor necrosis factor alpha pathways in erythroid cell apoptosis induced by human parvovirus B19. J. Virol. **73**: 8762–8770.
7. **Daeffler L, Horlein R, Rommelaere J, Nuesch JP.** 2003. Modulation of minute virus of mice cytotoxic activities through site-directed mutagenesis within the NS coding region. J. Virol. **77**: 12466–12478.

8. **Bergeron J, Menezes J, Tijssen P.** 1993. Genomic organization and mapping of transcription and translation products of the NADL-2 strain of porcine parvovirus. Virology **197**: 86–98.

9. **Zádori Z, Szelei J, Lacoste MC, Gariepy S, Raymond P, Allaire M, Nabi IR, Tijssen P.** 2001. A viral phospholipase A2 is required for parvovirus infectivity. Dev. Cell **1**: 291–302.

10. **Zádori Z, Szelei J, Tijssen P.** 2005. SAT: a late NS protein of porcine parvovirus. J. Virol. **79**(20): 13129–13138.

11. **Ozcan L, Tabas I.** 2012. Role of endoplasmic reticulum stress in metabolic disease and other disorders. Annu. Rev. Med. **63**: 317–328.

12. **Ellgaard L, Helenius A.** 2003. Quality control in the endoplasmic reticulum. Nat. Rev. Mol. Cell Biol. **4**: 181–191.

13. **Marciniak SJ, Ron D.** 2006 Endoplasmic reticulum stress signaling in disease. Physiol Rev. **86**(4): 1133–1149.

14. **Ron D, Hubbard SR.** 2008. How IRE1 reacts to ER stress. Cell. **132**(1): 24–26.

15. **Patil C, Walter P.** 2001. Intracellular signaling from the endoplasmic reticulum to the nucleus: the unfolded protein response in yeast and mammals. Curr Opin Cell Biol. **13**(3): 349–355.

16. **Kohno K.** 2010. Stress-sensing mechanisms in the unfolded protein response: similarities and differences between yeast and mammals. J Biochem. **147**(1): 27–33.

17. **Lee AH, Iwakoshi NN, Glimcher LH.** 2003. XBP-1 regulates a subset of endoplasmic reticulum resident chaperone genes in the unfolded protein response. Mol Cell Biol. **23**(21): 7448–7459.

18. **Shaffer AL, Shapiro-Shelef M, Iwakoshi NN, Lee AH, Qian SB, Zhao H., Yu X, Yang L, Tan BK, Rosenwald A, Hurt EM, Petroulakis E, Sonenberg N, Yewdell**

JW, Calame K, Glimcher LH, Staudt LM. 2004. XBP1, downstream of Blimp-1, expands the secretory apparatus and other organelles, and increases protein synthesis in plasma cell differentiation. Immunity. **21**(1): 81–93.

19. **Hinnebusch AG.** 2000. Mechanism and regulation of initiator methionyltRNA binding to ribosomes. p 185-243. *In* Sonenberg N, Hershey JWB, Mathews MB (ed). Translational Control of Gene Expression. CSHL Press: Cold Spring Harbor.

20. **Shi Y, Vattem KM, Sood R, An J, Liang J, Stramm L, Wek RC.** 1998. Identification and characterization of pancreatic eukaryotic initiation factor 2 alpha-subunit kinase, PEK, involved in translational control. Mol Cell Biol. **18**(12): 7499–7509.

21. **Harding HP, Zhang Y, Ron D.** 1999. Translation and protein folding are coupled by an endoplasmic reticulum resident kinase. Nature. **397**(6716): 271–274.

22. **Harding HP, Zhang Y, Zeng H, Novoa I, Lu PD, Calfon M, Sadri N, Yun C, Popko B, Paules R, Stojdl DF, Bell JC, Hettmann T, Leiden JM, Ron D.** 2003. An integrated stress response regulates amino acid metabolism and resistance to oxidative stress. Mol. Cell. **11**: 619–633.

23. **Wang X-Z, Lawson B, Brewer J, Zinszner H, Sanjay A, Mi L, Boorstein R, Kreibich G, Hendershot L, Ron D.** 1996. Signals from the stressed endoplasmic reticulum induce C/EBP homologous protein (CHOP/ GADD153). Mol Cell Biol. **16**: 4273–4280.

24. **Zinszner H, Kuroda M, Wang X, Batchvarova N, Lightfoot RT, Remotti H, Stevens JL, Ron D.** 1998. CHOP is implicated in programmed cell death in response to impaired function of the endoplasmic reticulum. Genes Dev. **12**(7): 982–995.

25. **Marciniak SJ, Yun CY, Oyadomari S, Novoa I, Zhang Y, Jungreis R, Nagata K, Harding HP, Ron D.** 2004. CHOP induces death by promoting protein synthesis and oxidation in the stressed endoplasmic reticulum. Genes Dev. **18**: 3066–3077.

26. **Bergeron J, Hébert B, Tijssen P**. 1996. Genome organization of the Kresse strain of porcine parvovirus: identification of the allotropic determinant and comparison with those of NADL-2 and field isolates. J Virol. **70**(4):2508-15.

27. **Hristov M, Erl W, Linder S, Weber PC.** 2004. Apoptotic bodies from endothelial cells enhance the number and initiate the differentiation of human endothelial progenitor cells in vitro. Blood. **104**(9):2761-6.

28. **Legrand C, Bour JM, Jacob C, Capiaumont J, Martial A, Marc A, Wudtke M, Kretzmer G, Demangel C, Duval D, et al.** 1992. Lactate dehydrogenase (LDH) activity of the cultured eukaryotic cells as marker of the number of dead cells in the medium [corrected]. J Biotechnol. **25**(3): 231–243.

29. **Goergen JL, Marc A, Engasser JM.** 1993. Determination of cell lysis and death kinetics in continuous hybridoma cultures from the measurement of lactate dehydrogenase release. Cytotechnology. **11**(3): 189–195.

30. **Korzeniewski C, Callewaert DM.** 1983. An enzyme-release assay for natural cytotoxicity. J Immunol Methods. **64**(3): 313–320.

31. **Terrinoni A, Ranalli M, Cadot B, Leta A, Bagetta G, Vousden KH, Melino G**. 2004. p73-alpha is capable of inducing scotin and ER stress. Oncogene. **23**(20): 3721–3725.

32. **Hübener J, Vauti F, Funke C, Wolburg H, Ye Y, Schmidt T, Wolburg-Buchholz K, Schmitt I, Gardyan A, Driessen S, Arnold HH, Nguyen HP, Riess O.** 2011. N-terminal ataxin-3 causes neurological symptoms with inclusions, endoplasmic

reticulum stress and ribosomal dislocation. Brain. **134**(Pt 7): 1925–42. doi: 10.1093/brain/awr118.

33. **Ngoh GA, Papanicolaou KN, Walsh K.** 2012. Loss of mitofusin 2 promotes endoplasmic reticulum stress. J Biol Chem. **287**(24): 20321–20332. doi: 10.1074/jbc.M112.359174.

34. **Iurlaro R, Muñoz-Pinedo C**. 2016. Cell death induced by endoplasmic reticulum stress. FEBS J. **283**(14):2640-52. doi: 10.1111/febs.13598.

35. **Herrada AA, Rojas-Colonelli N, González-Figueroa P, Roco J, Oyarce C, Ligtenberg MA, Lladser A.** 2012. Harnessing DNA-induced immune responses for improving cancer vaccines. Hum Vaccin Immunother. **8**(11):1682-93. doi: 10.4161/hv.22345.

36. **Marchini A, Bonifati S, Scott EM, Angelova AL, Rommelaere J.** 2015. Oncolytic parvoviruses: from basic virology to clinical applications. Virol J. **12**:6. doi: 10.1186/s12985-014-0223-y.

37. **Bär S, Daeffler L, Rommelaere J, Nüesch JP.** 2008. Vesicular egress of non-enveloped lytic parvoviruses depends on gelsolin functioning. PLoS Pathog. **4**(8):e1000126. doi: 10.1371/journal.ppat.1000126.

38. **Chen AY**, **Qiu J.** 2010. Parvovirus infection-induced cell death and cell cycle arrest. Future Virol. **5**(6): 731–743. doi:10.2217/fvl.10.56.

39. **Zhang H, Huang Y, Du Q, Luo X, Zhang L, Zhao X, Tong D.** 2015. Porcine parvovirus infection induces apoptosis in PK-15 cells through activation of p53 and mitochondria-mediated pathway. Biochem Biophys Res Commun. **456**(2):649–55. doi: 10.1016/j.bbrc.2014.12.011.

40. **Zhao X, Xiang H, Bai X, Fei N, Huang Y, Song X, Zhang H, Zhang L, Tong D.** 2016. Porcine parvovirus infection activates mitochondria-mediated apoptotic

signaling pathway by inducing ROS accumulation. Virol J. **13**:26. doi: 10.1186/s12985-016-0480-z.

41. **Fernandes S, Boisvert M, Szelei J, Tijssen P.** 2014. Differential replication of two porcine parvovirus strains in bovine cell lines ensues from initial DNA processing and NS1 expression. J Gen Virol. **95**(4):910-21. doi: 10.1099/vir.0.059741-0.

42. **Gupta SK, Sahoo AP, Rosh N, Gandham RK, Saxena L, Singh AK, Harish DR, Tiwari AK.** 2016. Canine parvovirus NS1 induced apoptosis involves mitochondria, accumulation of reactive oxygen species and activation of caspases. Virus Res. **213**: 46–61. doi: 10.1016/j.virusres.2015.10.019.

43. **Yoshida H, Matsui T, Yamamoto A, Okada T, Mori K.** 2001. XBP1 mRNA is induced by ATF6 and spliced by IRE1 in response to ER stress to produce a highly active transcription factor. Cell. **107**(7): 881–891.

44. **Kondratyev M, Avezov E, Shenkman M, Groisman B, Lederkremer GZ.** 2007. PERK-dependent compartmentalization of ERAD and unfolded protein response machineries during ER stress. Exp Cell Res. **313**(16): 3395–407.

45. **Hammadi M, Oulidi A, Gackière F, Katsogiannou M, Slomianny C, Roudbaraki M, Dewailly E, Delcourt P, Lepage G, Lotteau S, Ducreux S, Prevarskaya N, Van Coppenolle F.** 2013. Modulation of ER stress and apoptosis by endoplasmic reticulum calcium leak via translocon during unfolded protein response: involvement of GRP78. FASEB J. **27**(4): 1600–1609.

46. **Cleland WW.** 1964. Dithiothreitol, a New Protective Reagent for SH Groups. Biochemistry. **3**(4): 480–482.

47. **Lee DH, Goldberg AL.** 1998. Proteasome inhibitors cause induction of heat shock proteins and trehalose, which together confer thermotolerance in Saccharomyces cerevisiae. Mol Cell Biol. **18**(1): 30–38.

48. **Ali H, Christensen SB, Foreman JC, Pearce FL, Piotrowski W, Thastrup O.** 1985. The ability of thapsigargin and thapsigargicin to activate cells involved in the inflammatory response. Br J Pharmacol. **85**(3): 705–712.

49. **Boisvert M, Fernandes S, Tijssen P**. 2010. Multiple pathways involved in porcine parvovirus cellular entry and trafficking toward the nucleus. J Virol. **84**(15):7782-92. doi: 10.1128/JVI.00479-10.

50. **Yakinoglu A O, Heilbronn R, Burkle A, Schlehofer J, zur-Hausen H.** 1988. DNA amplification of adeno-associated virus as a response to cellular genotoxic stress. Cancer Res. **48**: 3123-3129.

51. **Yakobson B, Koch T, and Winocour E.** 1987. Replication of adeno-associated virus in synchronized cells without the addition of a helper virus. J. Virol. **61**: 972-981.

52. **Cornelis JJ, Su ZZ, Ward DC, Rommelaere J. 1981.** Indirect induction of mutagenesis of intact parvovirus H-1 in mammalian cells treated with UV light or with UV-irradiated H-1 or simian virus 40. Proc Natl Acad Sci U S A. **78**(7): 4480-4.

53. **Jordan R, Wang L, Graczyk TM, Block TM, Romano PR.** 2002. Replication of a cytopathic strain of bovine viral diarrhea virus activates PERK and induces endoplasmic reticulum stress-mediated apoptosis of MDBK cells. J Virol. **76**(19): 9588-99.

54. **Zhang L and Wang A.** 2012. Virus induced ER stress and the unfolded protein response. Front Plant Sci. **3**: 293. doi: 10.3389/fpls.2012.00293.

55. **Chan SW.** 2014. The unfolded protein response in virus infections. Front Microbiol. **5**: 518. doi: 10.3389/fmicb.2014.00518.

56. **Dash S, Chava S, Aydin Y, Chandra PK, Ferraris P, Chen W, Balart LA, Wu T, Garry RF.** 2016. Hepatitis C Virus Infection Induces Autophagy as a Prosurvival

744 Mechanism to Alleviate Hepatic ER-Stress Response. Viruses. **8**(5). pii: E150. doi:
745 10.3390/v8050150.
746 57. **Zhou Y, Qi B, Gu Y, Xu F, Du H, Li X, Fang W**. 2016. Porcine Circovirus 2
747 Deploys PERK Pathway and GRP78 for Its Enhanced Replication in PK-15 Cells.
748 Viruses. **8**(2). pii: E56. doi: 10.3390/v8020056.
749 58. **Schönthal AH.** 2012. Endoplasmic reticulum stress: its role in disease and novel
750 prospects for therapy. Scientifica (Cairo). **2012**:857516. doi: 10.6064/2012/857516.
751 59. **Yu YQ, Liu LC, Wang FC, Liang Y, Cha DQ, Zhang JJ, Shen YJ, Wang HP,**
752 **Fang S, Shen YX.** 2010. Induction profile of MANF/ARMET by cerebral ischemia
753 and its implication for neuron protection. J Cereb Blood Flow Metab. **30**(1): 79–91.
754 60. **Sano R, Reed JC.** 2013. ER stress-induced cell death mechanisms. Biochim Biophys
755 Acta. **1833**(12):3460–3470. doi: 10.1016/j.bbamcr.2013.06.028.
756 61. **Urra H, Dufey E, Lisbona F, Rojas-Rivera D, Hetz C.** 2013. When ER stress
757 reaches a dead end. Biochim Biophys Acta. **1833**(12): 3507-17. doi:
758 10.1016/j.bbamcr.2013.07.024.
759 62. **Han J, Back SH, Hur J, Lin YH, Gildersleeve R, Shan J, Yuan CL, Krokowski D,**
760 **Wang S, Hatzoglou M, Kilberg MS, Sartor MA, Kaufman RJ.** 2013. ER-stress-
761 induced transcriptional regulation increases protein synthesis leading to cell death. Nat
762 Cell Biol. **15**(5):481-90. doi: 10.1038/ncb2738.

763

764

765 **Legends**

766 Figure 1. The DNA and amino acid sequences of the wild type (A) and the SAT^{-} (B)
767 mutant Kresse strain (based on the U44978.1 sequence). The 2842^{th} and 2845^{th} nucleotides
768 were changed (T→A and T→C). These modifications did not change the amino acid

769 sequence of the VP1, however they led to a STOP codon in the SAT ORF and to the
770 substitution of the nearest methionine.
771
772 Figure 2. Spread of the wild type and the SAT^{-} mutant viruses in PT cells at a low
773 multiplicity (MOI: 0.01) infection. Infected cells (red) were visualized with the assembled
774 capsid specific 3C9 primary and CF594 labelled secondary antibody. (A) Cells were fixed in
775 the indicated time points and their nuclei were labelled with Hoechst 33342. (B) 3C9 antibody
776 was added to Kresse infected cells to monitor the inhibition of the secondary infections. The
777 beginning of the treatments is indicated on the pictures. The cells were fixed at 24 h p.i..
778
779 Figure 3. The change of the viral copy numbers during infection in the medium of PT
780 cells. (A) Copy numbers and infectious titer (indicated by triangles and columns respectively)
781 during low multiplicity (MOI: 0.01) infection. (B) Total copy numbers and copy numbers
782 measured after DNase treatment (represented by triangles and columns respectively) at high
783 multiplicity infection (MOI: 3). Error bars indicates standard deviation.
784
785
786 Figure 4. The different forms of the cells death during the PPV Kresse infection in
787 porcine testis cells. The error bars represent one standard deviation. (A) LDH activity in the
788 supernatant of the infected and control cells as indicator of the total cell death. Maximum
789 absorption value at 18 h p.i. (lysed control uninfected cells) are indicated by x. (B) The
790 attached cell count as indicator of the viability of cells. Number of uninfected cells at 24 h
791 represents 100%. (C) Rate of the attached propidium-iodide positive cells. (wt values were
792 calculated until 48 h p.i). (D) The rate of the attached pyknotic and karyorrhectic cells,

793 calculated by Hoechst staining. (wt values were calculated until 48 h p.i). (E) Swelling of
794 nuclei at at 22 h p.i.
795
796 Figure 5. Spreading of the PPV wild type and the SAT^{-} strains after ER stress inducer
797 treatments at low MOI (0.01) infection. Infected PT cells were fixed at 20 h p.i Monoclonal
798 3C9 anti-capsid antibody was used for the detection of the infected cells (red). Cell nuclei
799 (blue) were visualized by Hoechst staining. Concentration of the chemicals and the duration
800 of treatments (hours post infection) are indicated.
801
802 Figure 6. Changes of viral copy numbers in the medium at high multiplicity infection
803 (MOI: 3) after stress inducer treatments. All supernatants was harvested at 24 h p.i. (A) Cells
804 were infected with wild type and SAT^{-} strains and treated with ER stress inducers (MG132 20
805 μM and DTT 10 mM) during different time periods. (B) Cells were infected with wild type
806 and SAT^{-} strains and treated with UV-C light (sub-lethal) at different time points for a 5-
807 minute time period. (C). Infectious titer of the supernatants of differently treated infected
808 cells.
809
810 Figure 7. Morphological changes of the ER in PT cells during PPV infection. To
811 visualize the ER and the viral particles anti-calreticulin antibody (red) and anti-capsid (green)
812 anti-bodies were used, respectively.
813
814 Figure 8. Detection of ER stress protein markers during PPV infection. Cell nuclei
815 (blue) were visualized by Hoechst staining. (A) Activation of Xbp1 reversible ER stress
816 marker after wt and SAT^{-} strain infection. Xbp1 (green) and viral capsid (red) were labelled
817 with anti-Xbp1 and anti-capsid antibodies, respectively at 18 h p.i. (B) Activation of CHOP

irreversible ER stress marker after wt and SAT$^-$ strain infection. CHOP (green) and viral capsid (red) were labelled with anti-CHOP and anti-capsid antibodies, respectively at 24 h p.i. (C) Activation of Xbp1 in SAT$^-$ virus infected and non-infected cells at 60 h p.i. (D) Induction of the Xbp1 and CHOP after 20 μM MG132 treatment and sub-lethal UV treatment at 12 h.

Figure 9. Morphological changes of the ER in the SAT-DsRed fusion protein expressing PT cells. Cells were transfected with SAT-DsRed and as a control with DsRed (red) expressing plasmids. The calreticulin was labelled by anti-calreticulin monoclonal antibody (green) and the cell nuclei (blue) were visualized by Hoechst staining. The cells were fixed in different time points after transfection. Apoptotic nuclei are pointed out with arrows.

Figure 10. Localization of the porcine CHOP and its effect on the spreading of the SAT$^-$ virus strain. Viral capsid is labelled with anti-capsid antibodies (green) while nuclei (blue) are visualized by Hoechst staining. (A) Nuclear localization of the CHOP-DsRed fusion protein (red) in infected and non-infected cells. CHOP-DsRed expressing plasmids were transfected with wild type and pSAT$^-$ infectious clones or alone into PT cells and fixed at 24 h post transfection. (B) Cytopathic effect of the CHOP-DsRed at 18 h post transfection. Arrows indicate fragmented nuclei. (C) Spreading of the SAT$^-$ strain after co-transfection of the pSAT$^-$ infectious clone with CHOP-DsRed and SAT-DsRed expressing plasmids. As positive control, wild-type clone was transfected with DsRed expressing plasmid. Cells were fixed 96 h post transfection, blue (nucleus) and green (virus positive cells) channels were merged.

A. original sequence

DNA sequence 2820- ATGTGGAACAACACAACCCTAT**T**AA**T**GCAGGCACTGAATTGTCTGCAACAGGAA -2873

+1 Frame (VP1) V E Q H N P **I** **N** A S T E L S A T G

+2 Frame (SAT) M W N N T T L **L** **M** Q A L N C L Q Q E

B. mutated sequence

DNA sequence 2820- ATGTGGAACAACACAACCCTAT**A**AA**C**GCAGGCACTGAATTGTCTGCAACAGGAA -2873

+1 Frame (VP1) V E Q H N P **I** **N** A S T E L S A T G

+2 Frame (SAT) M W N N T T L **STOP** **T** Q A L N C L Q Q E

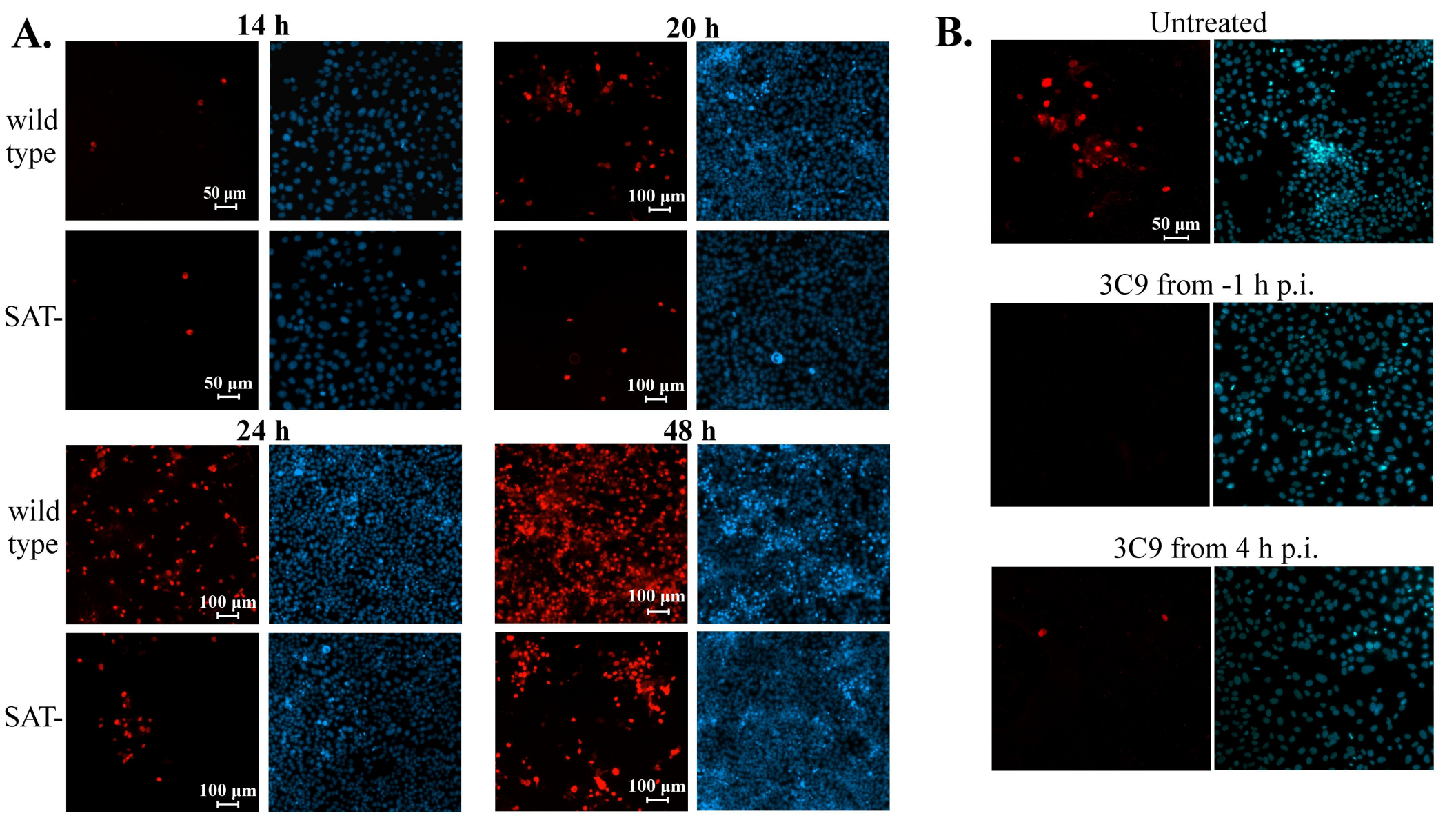
A.
14 h
20 h
wild type
SAT-
50 µm
100 µm
24 h
48 h
B.
Untreated
3C9 from -1 h p.i.
3C9 from 4 h p.i.

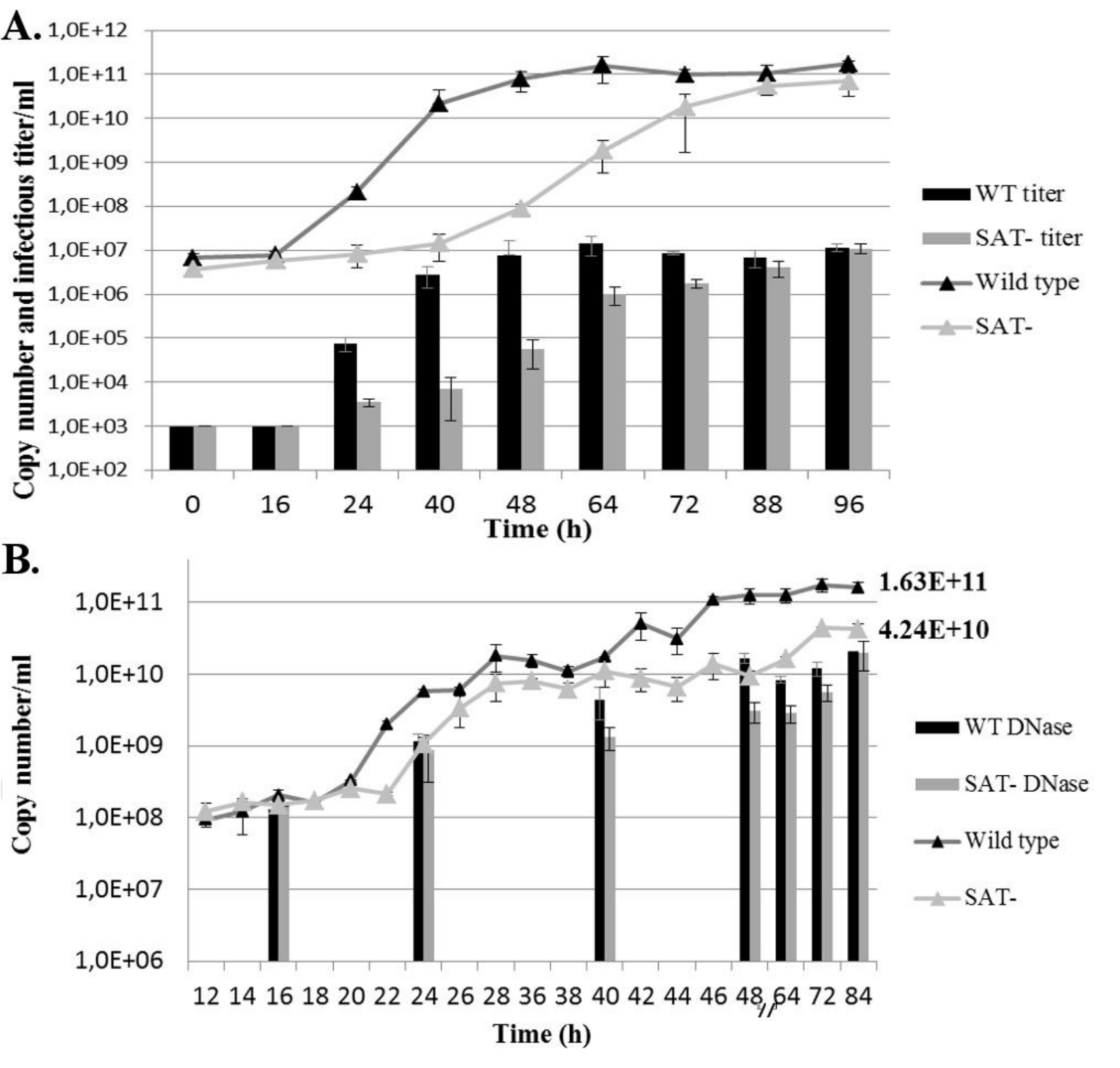
A.
Copy number and infectious titer/ml
1,0E+12
1,0E+11
1,0E+10
1,0E+09
1,0E+08
1,0E+07
1,0E+06
1,0E+05
1,0E+04
1,0E+03
1,0E+02
0
16
24
40
48
64
72
88
96
Time (h)
WT titer
SAT- titer
Wild type
SAT-
B.
Copy number/ml
1,0E+11
1,0E+10
1,0E+09
1,0E+08
1,0E+07
1,0E+06
1.63E+11
4.24E+10
12 14 16 18 20 22 24 26 28 36 38 40 42 44 46 48 64 72 84
Time (h)
WT DNase
SAT- DNase
Wild type
SAT-

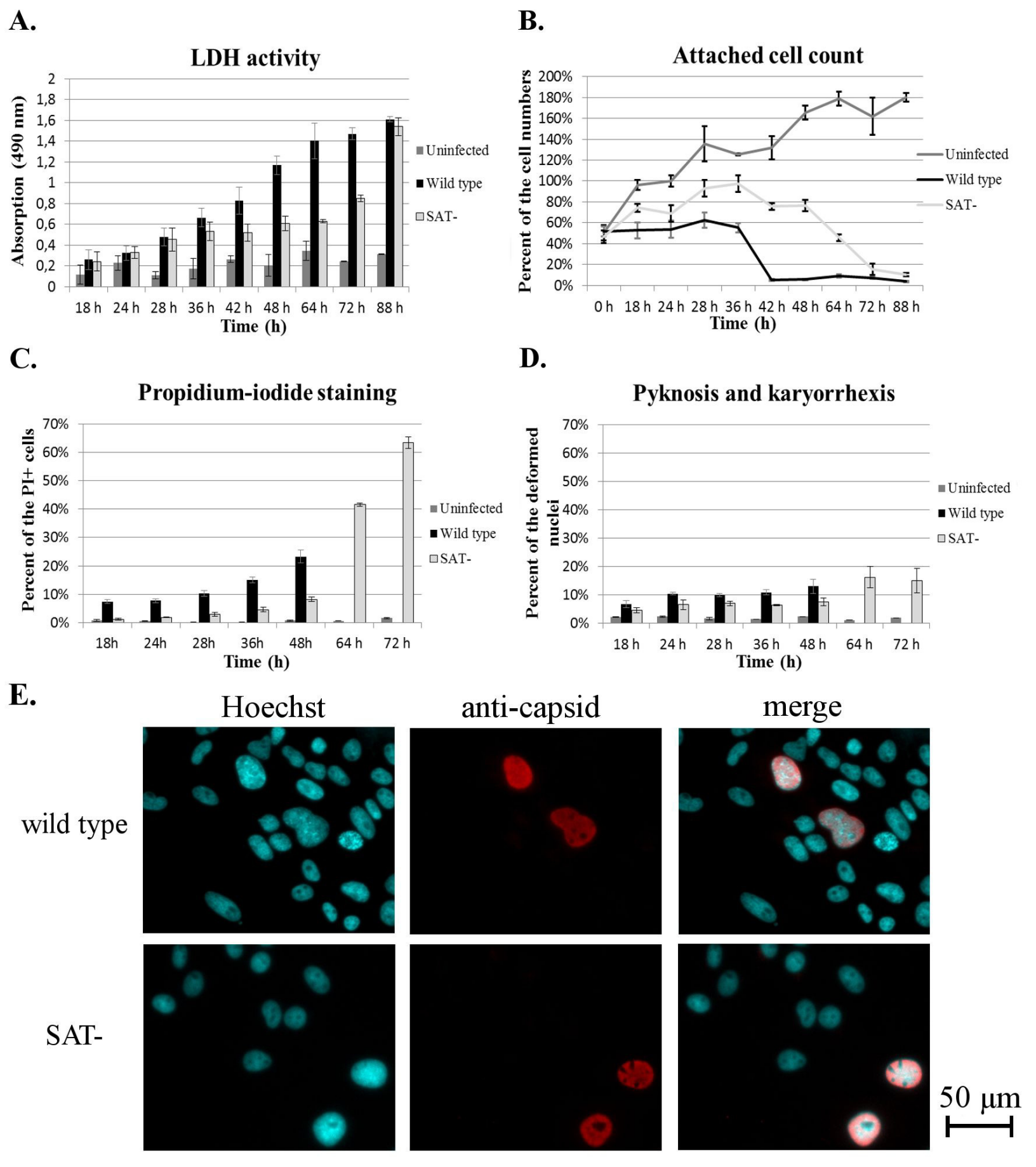
A.
LDH activity
Absorption (490 nm)
2
1,8
1,6
1,4
1,2
1
0,8
0,6
0,4
0,2
0
18 h
24 h
28 h
36 h
42 h
48 h
64 h
72 h
88 h
Time (h)
Uninfected
Wild type
SAT-
B.
Attached cell count
Percent of the cell numbers
200%
180%
160%
140%
120%
100%
80%
60%
40%
20%
0%
0 h
18 h
24 h
28 h
36 h
42 h
48 h
64 h
72 h
88 h
Time (h)
Uninfected
Wild type
SAT-
C.
Propidium-iodide staining
Percent of the PI+ cells
70%
60%
50%
40%
30%
20%
10%
0%
18h
24h
28h
36h
48h
64 h
72 h
Time (h)
Uninfected
Wild type
SAT-
D.
Pyknosis and karyorrhexis
Percent of the deformed nuclei
70%
60%
50%
40%
30%
20%
10%
0%
18 h
24 h
28 h
36 h
48 h
64 h
72 h
Time (h)
Uninfected
Wild type
SAT-
E.
Hoechst
anti-capsid
merge
wild type
SAT-
50 µm

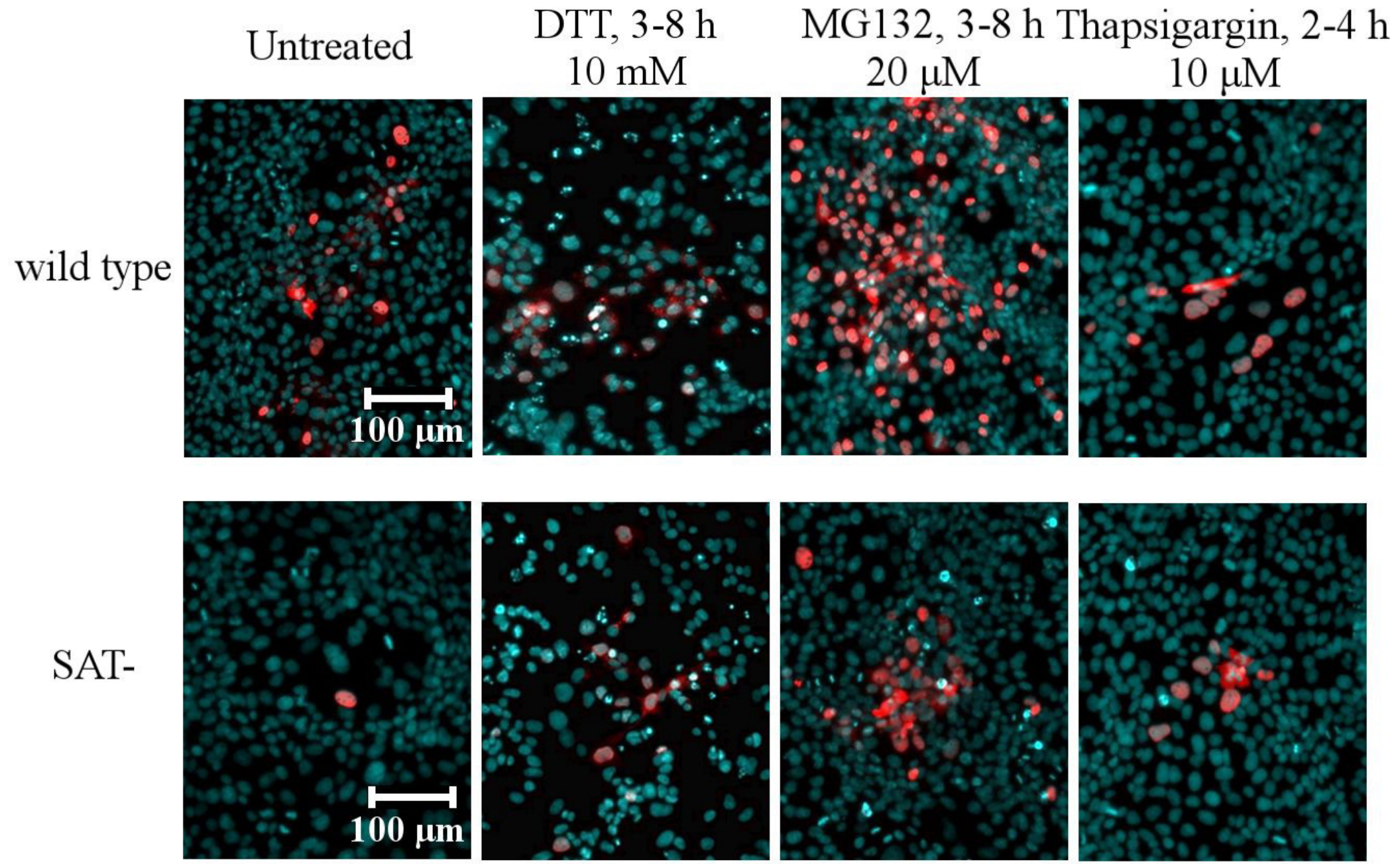
Untreated
DTT, 3-8 h
10 mM
MG132, 3-8 h
20 μM
Thapsigargin, 2-4 h
10 μM
wild type
SAT-
100 μm
100 μm

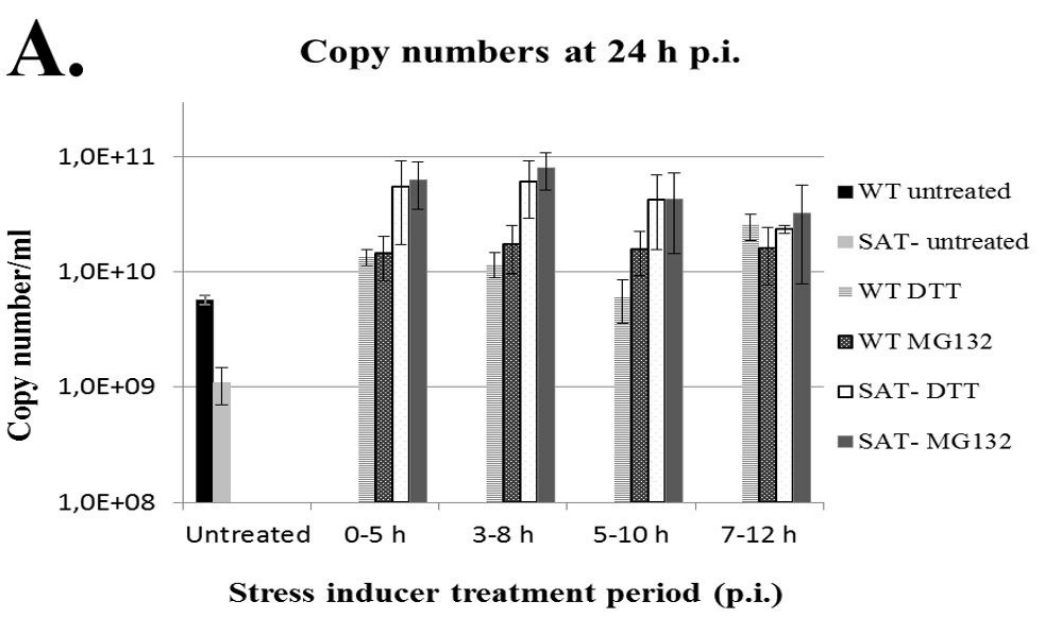
A.
Copy numbers at 24 h p.i.
1,0E+11
1,0E+10
1,0E+09
1,0E+08
Copy number/ml
WT untreated
SAT- untreated
WT DTT
WT MG132
SAT- DTT
SAT- MG132
Untreated
0-5 h
3-8 h
5-10 h
7-12 h
Stress inducer treatment period (p.i.)

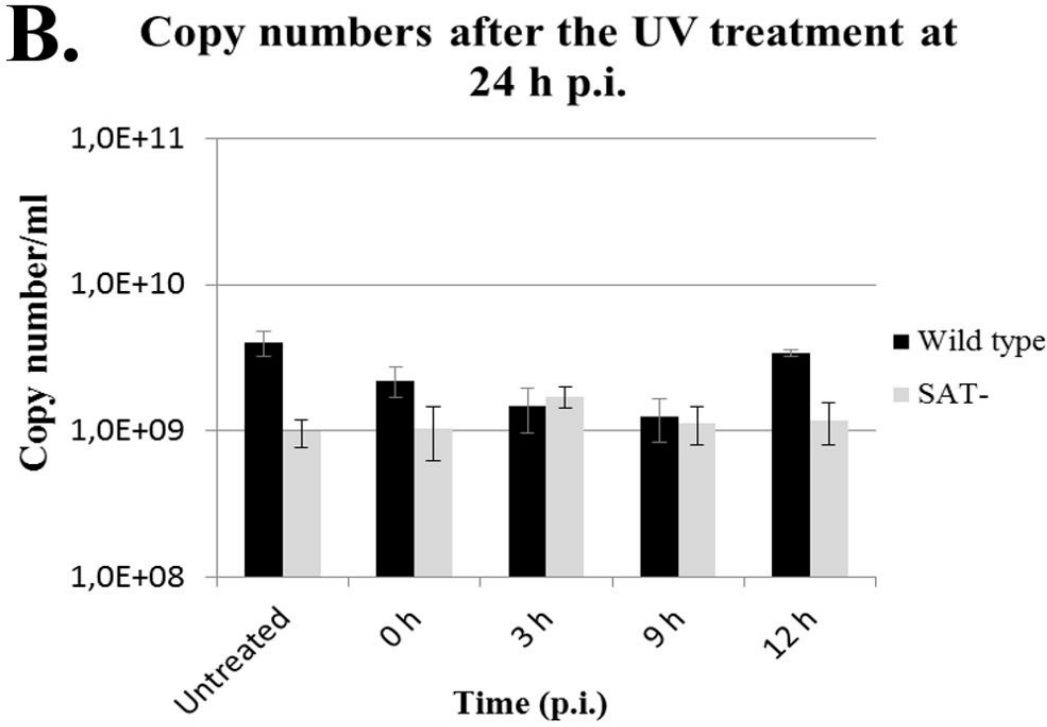
B.
Copy numbers after the UV treatment at 24 h p.i.
1,0E+11
1,0E+10
1,0E+09
1,0E+08
Copy number/ml
Wild type
SAT-
Untreated
0 h
3 h
9 h
12 h
Time (p.i.)

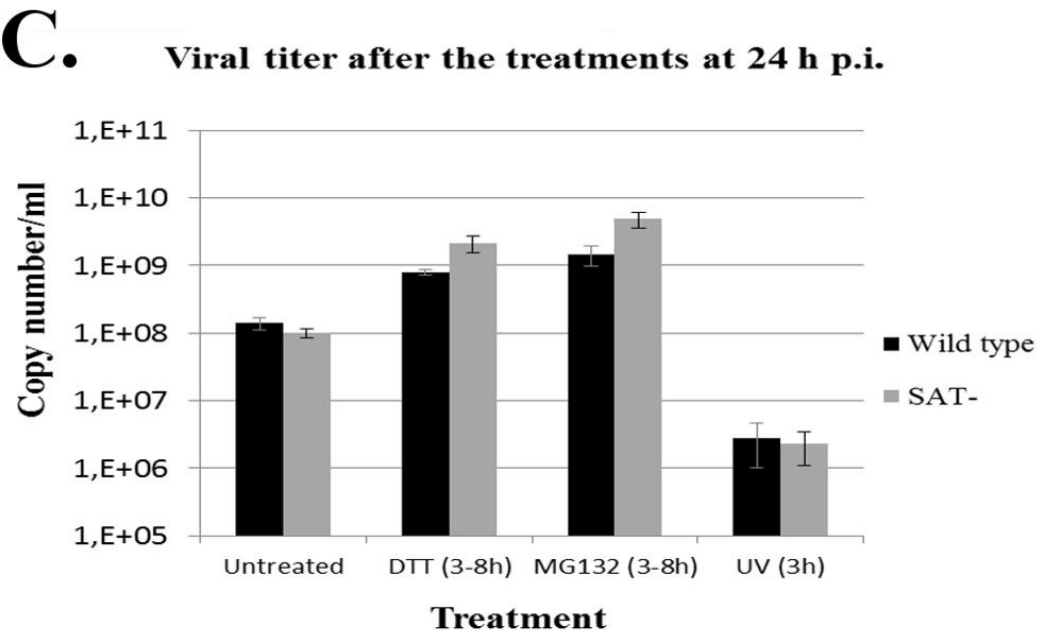
C.
Viral titer after the treatments at 24 h p.i.
1,E+11
1,E+10
1,E+09
1,E+08
1,E+07
1,E+06
1,E+05
Copy number/ml
Wild type
SAT-
Untreated
DTT (3-8h)
MG132 (3-8h)
UV (3h)
Treatment

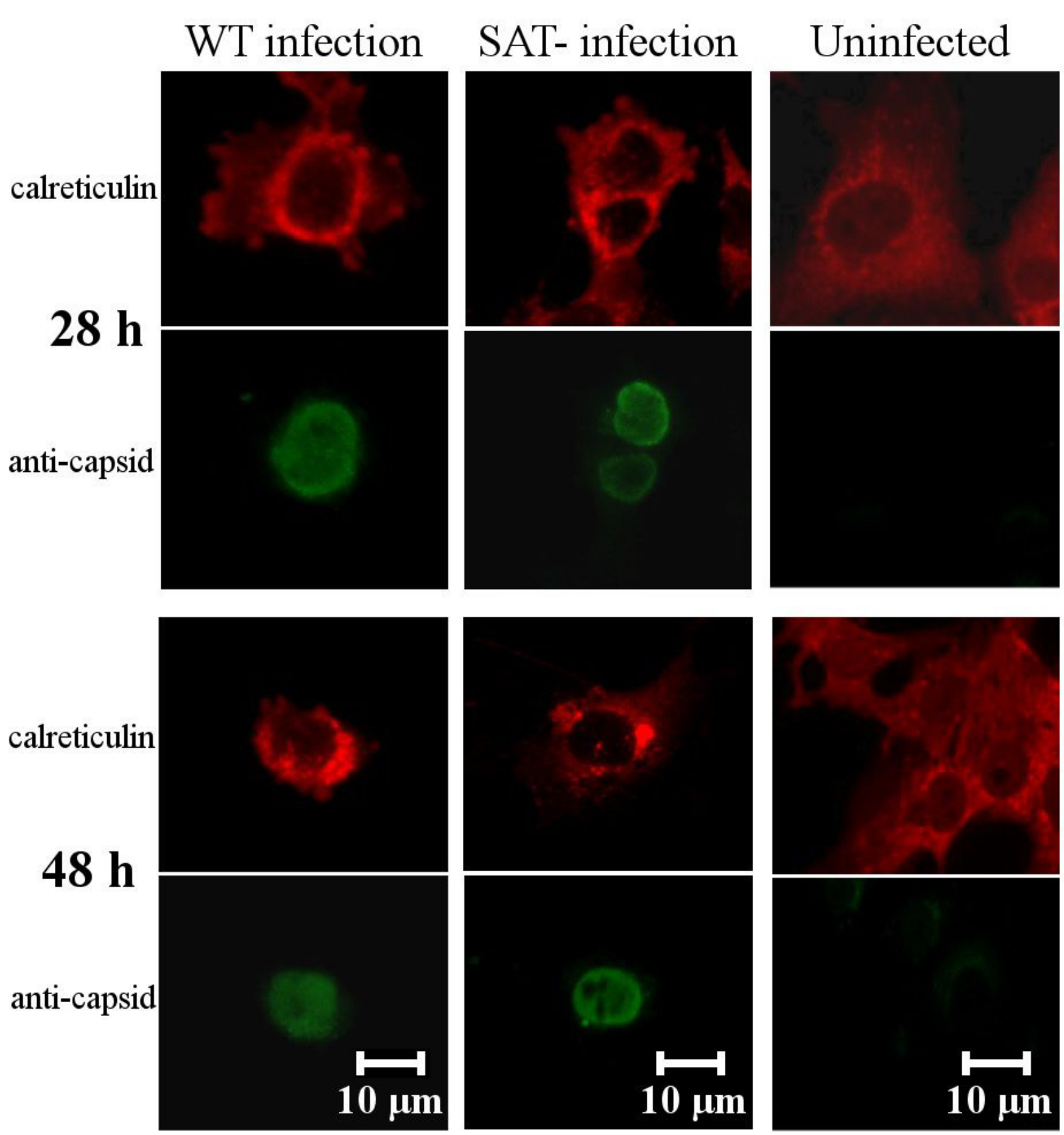
WT infection
SAT- infection
Uninfected
calreticulin
28 h
anti-capsid
calreticulin
48 h
anti-capsid
10 µm
10 µm
10 µm

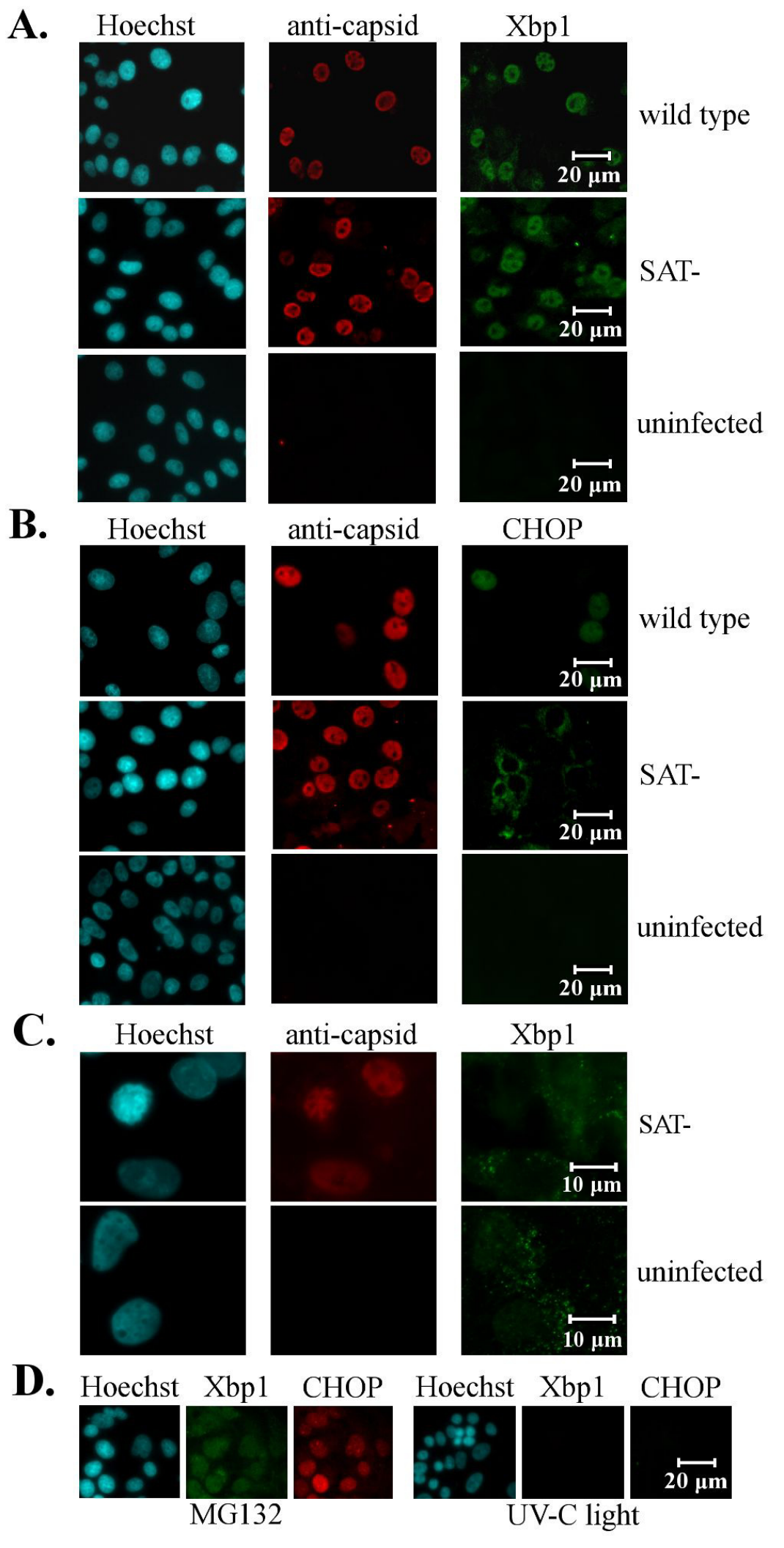
A.
Hoechst
anti-capsid
Xbp1
wild type
SAT-
uninfected
20 µm
B.
Hoechst
anti-capsid
CHOP
wild type
SAT-
uninfected
20 µm
C.
Hoechst
anti-capsid
Xbp1
SAT-
uninfected
10 µm
D.
Hoechst
Xbp1
CHOP
Hoechst
Xbp1
CHOP
20 µm
MG132
UV-C light

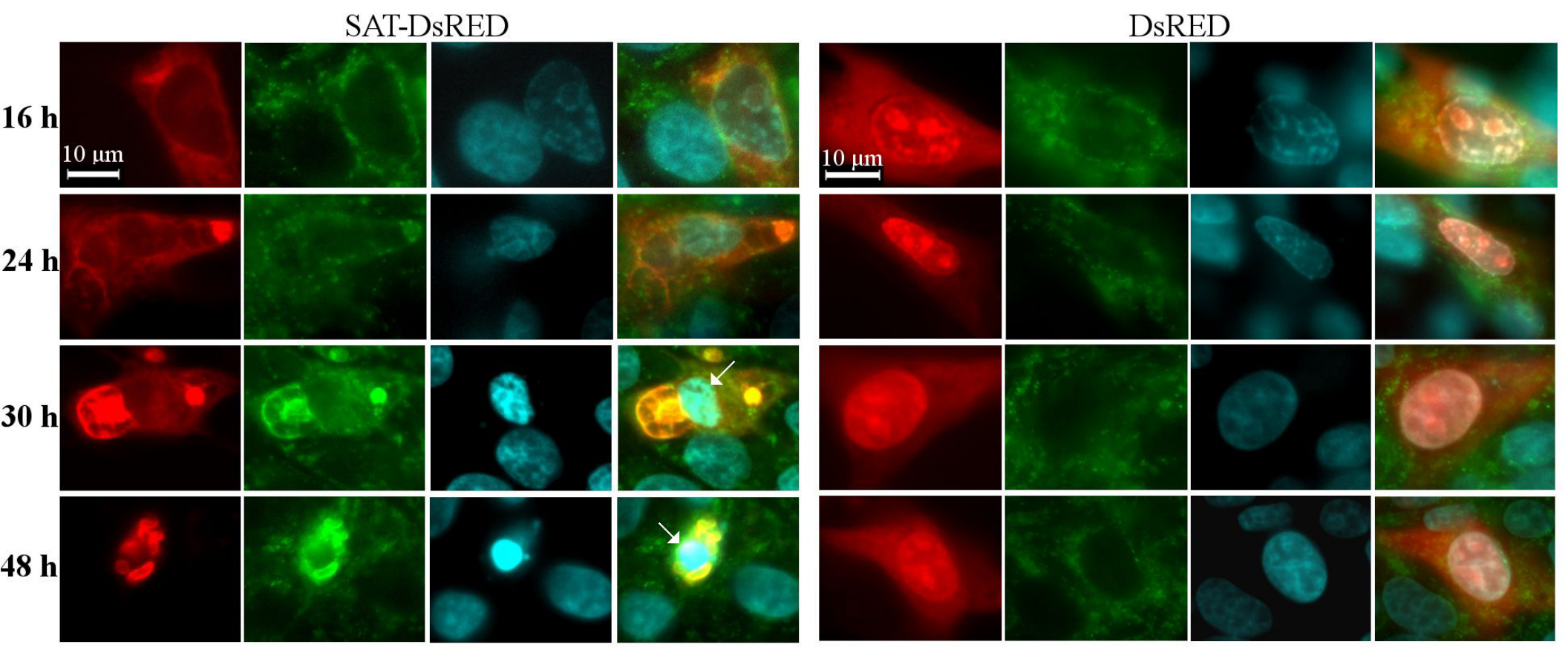
SAT-DsRED
DsRED
16 h
24 h
30 h
48 h
10 µm
10 µm

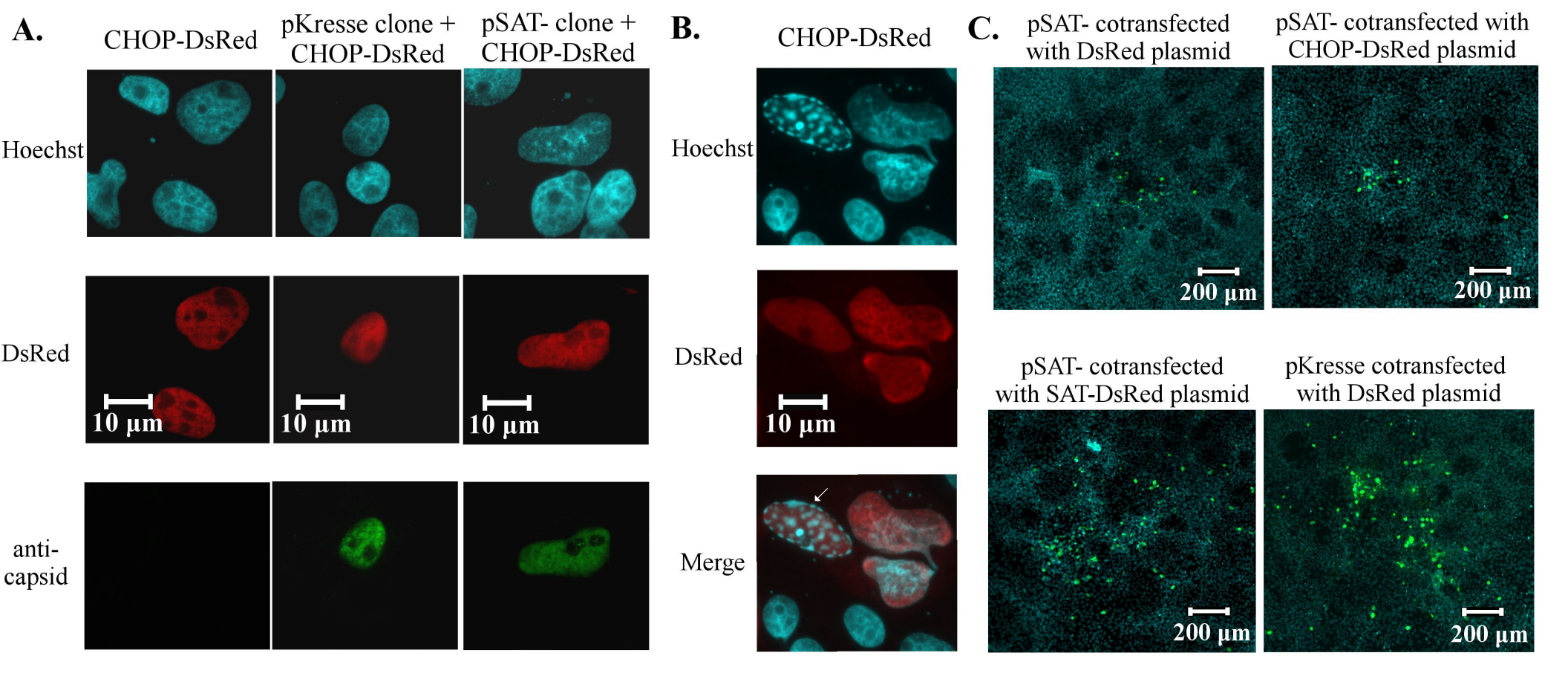
A.
CHOP-DsRed
pKresse clone + CHOP-DsRed
pSAT- clone + CHOP-DsRed
Hoechst
DsRed
anti-capsid
10 µm
10 µm
10 µm
B.
CHOP-DsRed
Hoechst
DsRed
Merge
10 µm
C.
pSAT- cotransfected with DsRed plasmid
pSAT- cotransfected with CHOP-DsRed plasmid
200 µm
200 µm
pSAT- cotransfected with SAT-DsRed plasmid
pKresse cotransfected with DsRed plasmid
200 µm
200 µm